

# Measurement of current profile dynamics in the Madison Symmetric Torus

S. D. Terry,<sup>a)</sup> D. L. Brower, and W. X. Ding

*Electrical Engineering Department, University of California, Los Angeles, California 90095*

J. K. Anderson, T. M. Biewer, B. E. Chapman, D. Craig, C. B. Forest, R. O'Connell, S. C. Prager, and J. S. Sarff

*Department of Physics, University of Wisconsin, Madison, Wisconsin 53706*

(Received 26 August 2003; accepted 20 November 2003)

The current profile and core magnetic field fluctuation amplitudes in a reversed-field pinch are measured by using a high-resolution polarimetry–interferometry system. This paper presents data showing a redistribution of the current during a sawtooth crash. Also, the core magnetic field fluctuation amplitude is observed to increase at a sawtooth crash consistent with the idea of nonlinearly driven dynamo current. In addition, the parallel current density increases in the outer region of the plasma during auxiliary pulsed parallel current drive. This was expected, as the external application of an edge parallel electric field is designed to flatten the current profile providing an equilibrium closer to the minimum energy Taylor state. However, the current density also increases in the core, relative to standard plasmas. This increase can be explained by a reduction of the dynamo (anti)current drive in the core that should accompany the measured reduction of magnetic fluctuations and by a drop in resistivity caused by the increased confinement of fast electrons. © 2004 American Institute of Physics. [DOI: 10.1063/1.1643917]

## I. INTRODUCTION

A significant challenge in creating a fusion reactor based on the reversed-field pinch (RFP) configuration is understanding and reducing the enhanced transport caused by large-amplitude magnetic tearing modes.<sup>1,2</sup> Since the stability of these modes is determined by radial gradients in the parallel current density profile, knowledge of this profile and its dynamics is crucial to any attempt to improve performance. Specifically, measurements of the current profile together with the magnetic field profile permit evaluation of the profile of the Taylor eigenvalue,<sup>3</sup>  $\lambda = J_{\parallel}/B$ , which determines tearing mode stability. A flat profile of  $\lambda$  is indicative of a stable plasma equilibrium.

While the current profile affects the stability of the magnetic fluctuations, fluctuations in the magnetic field can conversely affect the current profile through the dynamo.<sup>4</sup> Measurements<sup>5–7</sup> of dynamo quantities have confirmed that the parallel Ohm's law is balanced in the edge of RFP's if the magnetohydrodynamic (MHD) dynamo is included. This edge dynamo is particularly strong during the sawtooth crash, during which tearing mode amplitudes peak and core confinement drops. By using current profile modification techniques such as pulsed parallel (or poloidal) current drive (PPCD),<sup>8–11</sup> the equilibrium can be modified to be closer to a tearing stable state and the Taylor minimum energy state. When this is done, tearing mode amplitudes are observed to drop and confinement can increase by up to a factor of 10.

The multichord far-infrared (FIR) interferometer system on the Madison Symmetric Torus (MST)<sup>12</sup> has been upgraded to detect Faraday rotation with high time response. This capability enables the measurement of the toroidal cur-

rent and poloidal magnetic field profiles in the core of a reversed-field pinch plasma. The nonperturbative Faraday rotation measurements have up to 1  $\mu$ s time response and  $\approx 1$  mrad phase resolution. Due to the fast time response, not only can the temporal dynamics of the equilibrium profile be resolved, but direct measurement of core magnetic fluctuations also becomes possible. Measurements show an increase in the core magnetic field fluctuation amplitude during a sawtooth crash, followed by the flattening of the toroidal current profile to a more stable state. During PPCD, the  $\lambda = J_{\parallel}/B$  profile undergoes several changes. The overall profile flattens, while the current in the center peaks. The partial flattening returns the profile to a more stable state, while the core peaking is consistent with a reduction in the dynamo.

## II. RFP CURRENT PROFILE DYNAMICS

The reversed-field pinch configuration can be described as a minimum energy state satisfying Taylor's constraint of constant helicity.<sup>3</sup> In experiments, however, the equilibrium is observed to deviate from that predicted by helicity theory. A solution to the conserved helicity equation,

$$\nabla \times \mathbf{B} = \lambda \mathbf{B} \quad (1)$$

for the RFP in cylindrical geometry results in the equilibrium magnetic field profiles,

$$B_{\phi} = B_0 J_0(\lambda r), \quad (2)$$

$$B_{\theta} = B_0 J_1(\lambda r). \quad (3)$$

This solution requires that the eigenvalue  $\lambda = J_{\parallel}/B$  is constant in radius. However, due to the inherent magnetic shear in the RFP, the magnetic field in the edge (primarily in

<sup>a)</sup>Electronic mail: sterry@pppl.gov

the poloidal direction) is no longer aligned with the applied electric field (in the toroidal direction). Experimentally, therefore, the parallel current density, and  $\lambda$ , decreases in the edge. This deviation from the Taylor state provides a source of free energy for MHD instabilities such as tearing modes to form. These tearing modes can create magnetic islands and lead to stochastic field lines and enhanced transport.<sup>13</sup>

The observed phenomenon of the sawtooth in an RFP is hypothesized to result in the relaxation of the equilibrium closer to a Taylor state.<sup>4</sup> During these events,<sup>14</sup> toroidal flux increases while poloidal flux decreases. Central electron density drops and the edge density rises as core particle confinement degrades. Tearing mode fluctuation amplitudes increase to a value of 3–4% while the central electron temperature drops. The reversal parameter, defined as the ratio of the edge to the volume averaged toroidal magnetic field  $F \equiv B_\phi(a)/\langle B_\phi \rangle_V$ , becomes more negative. The pinch parameter, defined as the ratio of the edge poloidal field to the volume averaged toroidal field  $\Theta \equiv B_\theta(a)/\langle B_\phi \rangle_V$ , decreases. These reflect a flattening of the  $\lambda$  profile consistent with a move toward a Taylor minimum-energy state.

This dynamic can be understood as the relaxation of a resistively peaked current profile. If the plasma starts out in a tearing mode stable configuration, the parallel current density will be relatively flat in the central region and the toroidal magnetic field will be peaked and reversed in the edge. As the plasma evolves, the toroidal field will resistively dissipate while the current profile peaks in the center. These actions drive the equilibrium away from a flat  $\lambda$  profile and the minimum energy state. As some critical gradient in  $\lambda$  is reached, tearing instabilities develop. The dominant instabilities are core resonant and act to relax the plasma by flattening the current profile and converting poloidal flux into toroidal flux restoring the toroidal magnetic field. With the plasma back in a relaxed state, the cycle can begin anew.

The action of the tearing mode instabilities to relax the current profile is hypothesized to take the form of a dynamo. Many dynamo mechanisms, such as the Hall and MHD dynamos, have been proposed. Ohm's law, in a general form, can be written as

$$-\frac{m_e}{e^2 n_e} \frac{\partial \mathbf{J}}{\partial t} + \mathbf{E} + \mathbf{v} \times \mathbf{B} - \frac{1}{en_e} \mathbf{J} \times \mathbf{B} + \frac{\nabla P_e}{en_e} = \eta \mathbf{J}, \quad (4)$$

where  $m_e$  and  $e$  are the electron mass and charge,  $n_e$  is the electron density and  $P_e$  is the electron pressure. Taking a flux surface average, the parallel component becomes<sup>5</sup>

$$\eta J_\parallel - E_\parallel = \langle \tilde{\mathbf{v}} \times \tilde{\mathbf{b}} \rangle_\parallel + \frac{\langle \tilde{\mathbf{J}} \times \tilde{\mathbf{B}} \rangle_\parallel}{ne}, \quad (5)$$

where  $\sim$  refers to time varying quantities and density fluctuations have been neglected. The first term on the right-hand side of the equation is the MHD dynamo and the second term corresponds to the Hall dynamo. Thus fluctuations in the magnetic field, when correlated with either the velocity or current density fluctuations, can drive current along field lines. Experiment and MHD simulations show that the applied electric field cannot account for the driven current.<sup>15,16</sup> The core current is overdriven while the edge current is un-

derdriven. The dynamo is hypothesized to make up the difference. The dynamo would therefore drive antiparallel current in the core and parallel current in the edge, thereby acting to flatten the current profile.

During PPCD, auxiliary poloidal current is inductively driven in the edge of the plasma in order to locally flatten the parallel edge current.<sup>11</sup> This has been observed to result in the reduction in tearing mode fluctuation amplitude and a tenfold increase in energy<sup>17</sup> and particle<sup>18</sup> confinement. It has been shown computationally<sup>19</sup> that such auxiliary current drive can flatten the  $\lambda$  profile and stabilize the core resonant tearing modes. The reduction in tearing mode activity would lead to a decrease in the dynamo current, possibly causing the current profile to peak.

The hypothesis of the MHD dynamo acting to relax the plasma during the sawtooth event has been confirmed in the edge of MST with probe measurements<sup>5–7</sup> (although measurements at smaller radii are underway to explore other dynamo mechanisms). However, core measurements of the current profile and magnetic field fluctuations until now were unavailable. The recent upgrade of the far-infrared interferometer/polarimeter on MST provides for measurements of these quantities in the core with high temporal resolution.

### III. EXPERIMENTAL SETUP

Interferometric measurements on MST are made using a vertically viewing 11 chord FIR system.<sup>20,21</sup> A CO<sub>2</sub> laser with nominal output power of 140 W drives two FIR laser cavities at a wavelength of 432.5  $\mu\text{m}$  (694 GHz). The two cavities are typically operated at a difference frequency of 750 kHz. The combined signal from the beams is sampled at a rate of 1 MHz. Because of aliasing, this results in a heterodyne signal at 250 kHz. The time resolution is thus set at 4  $\mu\text{s}$ . By digitizing at a higher rate and removing the aliasing, it is possible to obtain time resolution up to 1  $\mu\text{s}$ .

The upgrade of the interferometer on MST to include a polarimetry capability utilizes two colinear counter-rotating circularly polarized beams as probes to measure the Faraday rotation.<sup>22</sup> As each beam travels through the plasma, it experiences a phase shift related to the product of the electron density and the component of the magnetic field parallel to the beam. Half the difference in phase between the two beams gives the Faraday rotation angle,  $\Psi$ , where

$$\Psi = \frac{\lambda^2 e^3}{8\pi^2 c^3 \epsilon_0 m_e^2} \int n_e B_\parallel dl = 2.62 \times 10^{-13} \lambda^2 \int n_e B_\parallel dl, \quad (6)$$

where  $B_\parallel$  is the parallel (poloidal) component of the magnetic field,  $n_e$  is the electron density, and  $\lambda$  is the FIR wavelength, all in MKS units. Since the electron density profile is known from interferometer measurements, the Faraday rotation can be used to determine the line-integrated poloidal magnetic field. By using a fitting technique and Ampère's law, the toroidal current profile can then be determined.

The two probe beams are split between 11 chords by wire mesh beam splitters and pass through the plasma. The signal, which is measured at the difference frequency of the

lasers, is then digitized and the phase computed using a digital phase comparator technique.<sup>23</sup> A third reference beam is required to obtain simultaneous density information. However, the system as presently configured is limited to two beams. In order to obtain the density profile necessary to extract the magnetic field information from the Faraday rotation signal, the system must be operated in the interferometry mode with one beam propagating through the plasma and one acting as a local oscillator.<sup>20,21</sup> For the data presented in this paper, an ensemble of approximately 150 shots was taken with the system in each mode. The shots were selected for inclusion in the ensemble based on their closeness to a defined standard for certain machine parameters such as plasma current and density. The two sets of data were then combined in order to determine the toroidal current profile. All measurements were made on the Madison symmetric torus, a reversed field pinch with major radius  $R_0 = 1.5$  m and minor radius  $a = 0.51$  m. The data shown in this paper were taken during discharges using deuterium as a fill gas with a plasma current of 385 kA and a line-averaged density of  $\approx 1 \times 10^{13} \text{ cm}^{-3}$ .

One important issue which must be addressed is the conservation of beam polarization. The wire mesh beamsplitters used at these frequencies are anisotropic in their reflection and transmission properties. As the FIR beam propagates through the meshes, the polarization is modified. This results in a nonlinear response of the measured polarization angle to the actual change in polarization as the beam propagates through the plasma. In order to obtain the correct Faraday rotation angle, this response must be measured and used to calibrate the measured data.<sup>24</sup>

The measured Faraday rotation angle is equal to the line integral of the product of the electron density and the poloidal magnetic field. Therefore, changes or fluctuations in the Faraday rotation can be caused by either density or magnetic field fluctuations. By expanding the Faraday rotation angle, the magnetic field parallel to the FIR beam (the  $z$  direction), and the density to first order,

$$\Psi = \Psi_0 + \tilde{\Psi},$$

$$B_z = B_{0z} + \tilde{B}_z,$$

$$n = n_0 + \tilde{n},$$

the fluctuating Faraday rotation angle can be written as

$$\tilde{\Psi} = c_f \left( \int B_{0z} \tilde{n} dz + \int \tilde{B}_z n_0 dz \right), \quad (7)$$

where  $\sim$  refers to a fluctuating quantity and the subscript 0 refers to an equilibrium quantity. This equation shows that fluctuations in  $\Psi$  are given by the sum of the fluctuating electron density weighted by the equilibrium magnetic field and the fluctuating magnetic field weighted by the equilibrium density.

However, for fluctuations with poloidal mode number  $m = 1$ , the density fluctuations and  $B_{0z} dz$  are zero for a chord through the magnetic axis. This means that the first term on the right-hand side of Eq. (7) is zero, and thus fluctuations at the  $m = 1$  frequencies ( $> 5$  kHz) measured on this

chord are due to perturbations of the magnetic field. We can therefore measure the line-integrated amplitude of the component of the magnetic perturbation along chords that pass near the magnetic axis.<sup>25</sup> In this case, the component measured is in the radial direction. Since this line integral is weighted by the density profile, which is peaked in the core, and by the radial magnetic field fluctuation profile, which goes to zero at the wall, the measurement has the most sensitivity in the core. Therefore, to a good approximation, the fluctuations on the central chords can be considered to be core radial magnetic field fluctuations. Further confirmation of this is given by measurements of the phase and amplitude of the fluctuations.<sup>25</sup>

#### IV. EXPERIMENTAL METHOD

While the density profile can be determined from the interferometer data by Abel inversion,<sup>26</sup> the poloidal magnetic field is obtained from the Faraday rotation data by using a fitting method. In this section, we describe two methods used to determine the poloidal magnetic field profile from the combined interferometer and polarimeter data. The first involves a parametrized fit of a poloidal field profile to the Faraday rotation data. The second is a Grad–Shafranov equilibrium solver, MSTFIT,<sup>27</sup> which uses data from the full set of MST diagnostics. Once this profile is determined, we can calculate the toroidal current and electric field profiles.

The MSTFIT code calculates a Grad–Shafranov equilibrium constrained to fit multiple diagnostic inputs. The resulting fit provides flux surface averaged profiles for many different experimental quantities such as the parallel current density  $J_{\parallel}$ ,  $q = (r/R)(B_{\phi}/B_{\theta})$ , and  $\lambda$ . However, the time resolution of the fits is limited by the time resolution of the input data. Thus, profiles can only be obtained at time scales of roughly 250  $\mu\text{s}$  (limited by other diagnostics such as motional Stark effect and Thomson scattering), which is significantly slower than the time resolution of the Faraday rotation data.

The parameterized fit method only takes the interferometer, polarimeter, and total plasma current data as inputs. The fits therefore can be generated on the time scale of  $\approx 4 \mu\text{s}$ . The resulting profiles are limited to the poloidal magnetic field and toroidal current density components, however. The toroidal current density is assumed to have the form

$$J_{\phi}(r) = \alpha_1 \left( 1 - \left( \frac{r}{a} \right)^2 \right)^{\alpha_2}, \quad (8)$$

where  $\alpha_1$  and  $\alpha_2$  are free parameters and  $a$  is the minor radius. A third free parameter identifies the location of the magnetic axis which is largely determined by the point in space where the Faraday rotation equals zero. Using other trial functions had no large effect on the shape of the fitted current density profile for standard and PPCD shots. The flux surface geometry is approximated as nested circles with a Shafranov shift which varies as a function of radius. For a given set of parameters, the poloidal magnetic field in the cylindrical approximation can be determined using Ampère’s law,

$$\mu_0 J_\phi(r) = \frac{1}{r} \frac{d[rB_{\theta,\text{cyl}}(r)]}{dr}. \quad (9)$$

Toroidal curvature effects are included under the large aspect ratio expansion as

$$B_\theta(r) = B_{\theta,\text{cyl}} \left[ 1 - \left( \frac{r}{R_0} + \frac{d\delta(r)}{dr} \right) \cos \theta \right], \quad (10)$$

where  $R_0$  is the major radius and  $\delta(r)$  is the Shafranov shift as a function of radius. The poloidal field profile in conjunction with the density profile can then be used to calculate the Faraday rotation on each chord. The fitting routine then finds the set of parameters which minimizes the deviation from the measured polarimetry data and total toroidal current.

For the data shown in this paper, the parametrized fit routine was used to determine the toroidal current and poloidal magnetic field profiles. The parametrized fit is validated by the more accurate full reconstruction, allowing it to reliably be used to measure time variations. Profiles for  $q$ ,  $\lambda$  and parallel current were determined using MSTFIT. Figure 1 shows a comparison between the outputs of each code for the same shot. The raw Faraday rotation data is shown in Fig. 1(a). Both codes are able to fit the raw data well. The toroidal current and poloidal field profiles that correspond to those fits for each code are shown in Figs. 1(b) and 1(c). Both codes show a good agreement between their output profiles for the toroidal current and poloidal magnetic field. In a sense this is not surprising as each code uses a least squares fitting routine to determine the current profiles. However, the flux surface geometry used by MSTFIT is more complex and, since it is a solution to the Grad–Shafranov equation, should be closer to the true experimental geometry. The fact that the functional fit code can find almost the same toroidal current profile means that the nested circular flux surface approximation is valid.

## V. EXPERIMENTAL RESULTS

### A. Sawtooth crash

A dataset was taken on MST during standard sawtooth discharges with a plasma current of 385 kA. By ensembling the data relative to each sawtooth crash (approximately 400 events), we are able to obtain a flux-surface average and measure the change in the plasma parameters during the entire cycle. Specifically, from the Faraday rotation measurements, we can determine the toroidal current and poloidal magnetic field profiles. Through equilibrium modelling with MSTFIT, we can also generate the  $\lambda$ ,  $J_\parallel$  and  $q$  profiles.

The ensembled Faraday rotation signals from all 11 of the polarimeter chords are shown in Fig. 2. The sawtooth event shows up clearly on all of the chord traces. Since the measured Faraday rotation angle is due to the product of the density and magnetic field, the change during the sawtooth cycle can correspond to changes in either component, or both. For example, on the outermost chords, the absolute phase change increases corresponding to an increase in the density, for the most part, at the location of those chords. The chords nearer the plasma center show a decrease in the ab-

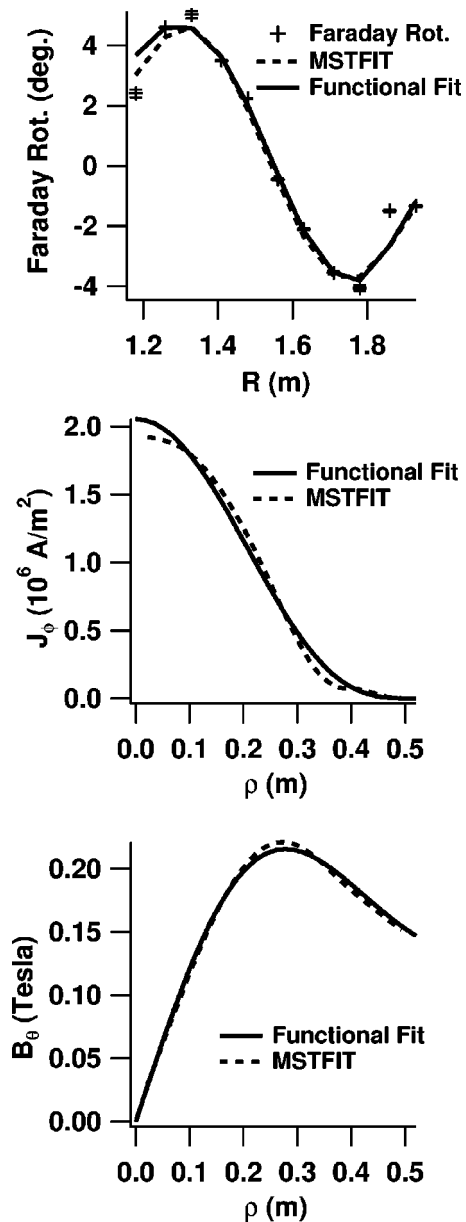


FIG. 1. The calculated fits to the raw Faraday rotation data, toroidal current and poloidal magnetic field profiles from the parametrized fit and MSTFIT.

solute phase change. As shown below, this is due to a decrease in the poloidal magnetic field in the plasma core.

The drop in current density on axis during the sawtooth crash, as determined by several models, is shown in Fig. 3(a). This correlates in time with an increase in magnetic fluctuation amplitude shown in Fig. 3(a). Data is presented from the alpha model,<sup>28</sup> a cylindrical equilibrium model based on a Taylor state with the plasma  $\beta \equiv nkT/B^2/2\mu_0$  treated as a free parameter, the slope model (which finds the on axis current from the derivative of the Faraday rotation data near the axis),<sup>29</sup> and the functional fit to the polarimetry data. Note that the alpha model does not include polarimetry data but only uses the parameters  $F$  and  $\theta$ . All models show an approximately 20% decrease in the on-axis current.

By following the toroidal current density profile evolution over a sawtooth crash, the flattening of the profile can be

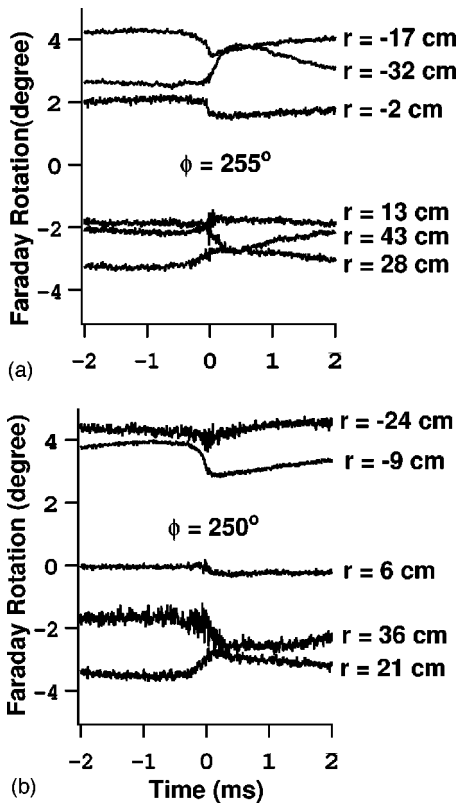


FIG. 2. The raw Faraday rotation signal traces for 11 chords. (a) shows the chords located at toroidal angle 255° and (b) shows chords at toroidal angle 250°.

seen as shown in Fig. 4. Figure 5 shows the change in toroidal current and poloidal magnetic field from 0.25 ms before the crash to 0.25 ms after the crash. The toroidal current is observed to decrease in the core from a peak value of  $2 \text{ MA m}^{-2}$  to roughly  $1.6 \text{ MA m}^{-2}$  consistent with the poloidal field decreasing in the core of the plasma after the sawtooth crash. The parallel current and  $\lambda$  profiles as determined by MSTFIT are shown in Fig. 6. The parallel current decreases in the core and increases in the edge after the sawtooth event. Most significantly, the  $\lambda$  profile is flattened after the crash. Figure 7 shows an increase of  $q$  on axis after the crash combined with a decrease of  $q$  at the edge. Figure 8 is a surface plot of the parallel current,  $J_{\parallel}$ , as a function of space and time relative to the sawtooth crash. The on-axis current decreases while more current is driven at the edge as the plasma evolves through the crash.

The evolution of the plasma profiles over the sawtooth crash supports the picture of a sawtooth crash being a relaxation event. The poloidal field profile is observed to decrease corresponding to a decrease in poloidal flux. This is consistent with the idea that poloidal flux is converted to toroidal flux by the sawtooth crash. The flattening of the current and  $\lambda$  profiles suggests that the RFP is relaxing to a state more stable to tearing fluctuations. The increase in  $q$  on axis and the decrease on the edge shows that the equilibrium field is becoming more deeply reversed after the crash. This suggests that the sawtooth crash acts against field diffusion to maintain the reversed equilibrium by generating toroidal flux.

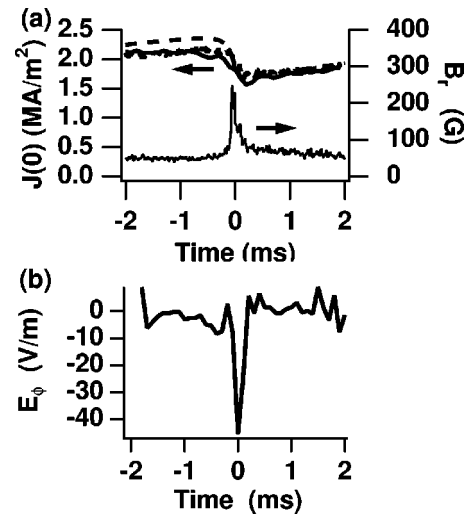


FIG. 3. The amplitude of the radial magnetic field fluctuations increases at the sawtooth crash corresponding with a drop in on-axis current. (a) shows the line averaged fluctuation amplitude as measured from the Faraday rotation signal on a chord passing through the magnetic axis. As such, it primarily measures  $\bar{B}_r$ . (a) also shows a drop in on-axis current as determined from the functional fit code (solid trace), the alpha model (dashed), and the slope model (dotted). (b) shows an increase in the on-axis toroidal electric field at the sawtooth crash calculated from the fit of the poloidal magnetic field profile to the polarimetry data.

Since we measure the poloidal field profile as a function of time, we can calculate the time-varying toroidal electric field profiles in MST by using Faraday's law. The toroidal electric field as a function of radius is given by

$$E_{\phi}(r) = \frac{V_{pg}}{2\pi R_0} - \int_r^a \frac{dB_{\theta}(r')}{dt} dr', \quad (11)$$

where  $V_{pg}$  is the voltage measured at the insulating poloidal gap (vertical cut) in the vacuum vessel and  $R_0$  is the major radius. We calculate the poloidal magnetic flux at each time point and take the derivative with respect to time. This allows the calculation of the toroidal electric field profile at each time point. Figure 3(b) shows the toroidal electric field

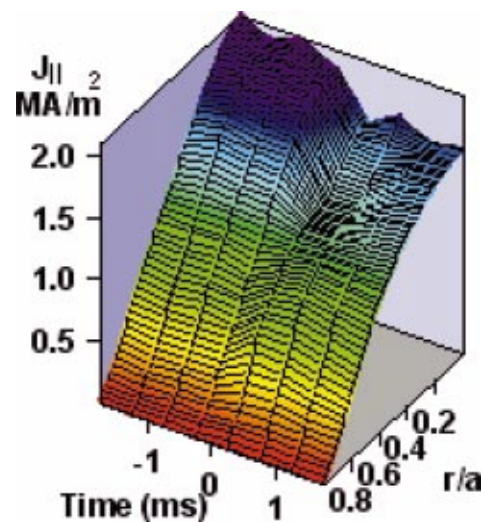


FIG. 4. (Color) The toroidal current profile flattens after a sawtooth crash.

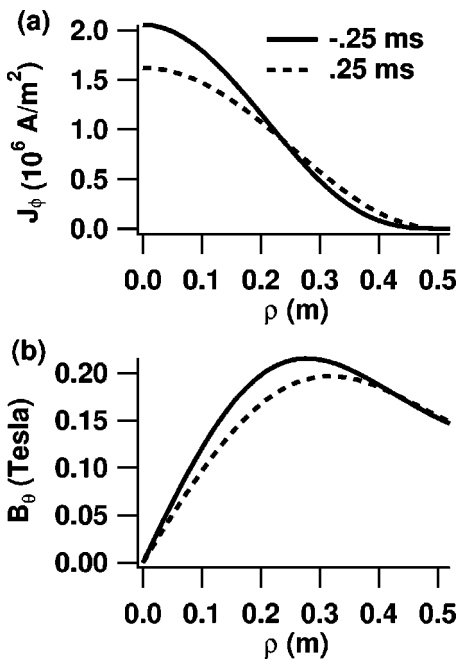


FIG. 5. The (a) toroidal current, and (b) poloidal magnetic field profiles before and after a sawtooth crash.

on axis during a sawtooth crash. The  $E$  field strength increases sharply at the sawtooth crash. This is also the time at which the dynamo electric field, as inferred from measured magnetic and velocity fluctuations in the edge, is at its peak. In order to explain the observed electric field increase in the core, there would need to also be an increase in magnetic fluctuation amplitude in the core. Of course, a quantitative measurement of the dynamo electric field would require

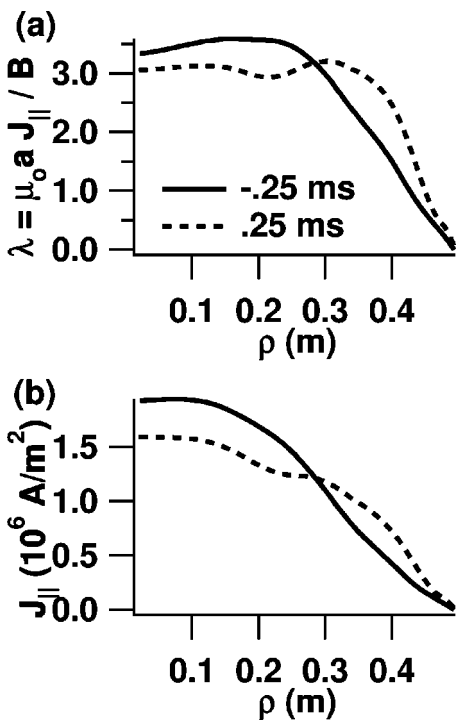


FIG. 6. The (a)  $\lambda = (J \cdot B / B^2)$  and (b) parallel current profiles before and after a sawtooth crash.

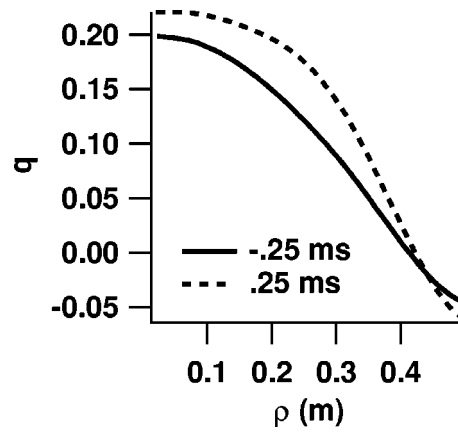


FIG. 7.  $q$  on axis and throughout most of the plasma volume increases after the crash, though it decreases in the edge.

other fluctuation measurements as well. However, the correlation of electric field and magnetic fluctuation amplitude in time would be strongly suggestive of a causal link. Figure 3(a) shows the line averaged fluctuation amplitude of the radial magnetic field as measured on the chord passing through the magnetic axis. Analogously to the edge fluctuation measurements made by probes or external magnetic pickup coils, the amplitude of  $\tilde{B}_r$  is observed to increase in the core at the crash. Thus, the data supports the hypothesis that a strongly antiparallel dynamo electric field is driven in the core by increased core fluctuations.

**B. Pulsed parallel current drive**

The point of auxiliary poloidal current drive in MST is to create a more stable profile of the Taylor eigenvalue  $\lambda$  leading to an equilibrium with improved stability to tearing modes. Experimentally, this is indicated by the drop in tearing mode amplitude as measured by external magnetic pickup coils and the increase in confinement. It can also be seen in the plot of the  $\lambda$  value in Fig. 9. For the PPCD case, the region of high  $\lambda$  gradient, which begins at  $r = 0.25$  m in a standard discharge, is moved outward in radius ( $t = 13.5$  ms), leaving a relatively flat region over more of the plasma volume. The reduced  $\lambda$  gradient should lead to a reduction in tearing mode amplitude. The Faraday rotation measurement of line-integrated  $m = 1$  radial magnetic fluctuation amplitude in the core (Fig. 10) also drops during PPCD. This is consistent with a decrease in magnetic fluctuation amplitudes across the plasma leading to good flux surfaces and a decrease in stochastic transport. Later in time (15 ms), the  $\lambda$  profile also increases in the core, indicating the parallel current is increasing in that region.

Figure 11 shows the toroidal current, parallel current, and poloidal field profiles during PPCD and compares it to the profile at 0.25 ms before a sawtooth crash. The data was taken from an ensemble of PPCD shots where the enhanced confinement period extended from 9 to 20 ms. The current drive ends at  $\approx 15$  ms, which also corresponds to the time of the peak core electron temperature. The PPCD profiles shown are measured at 15.5 ms. Both the toroidal and parallel current profiles show an increase in the core current. Sev-

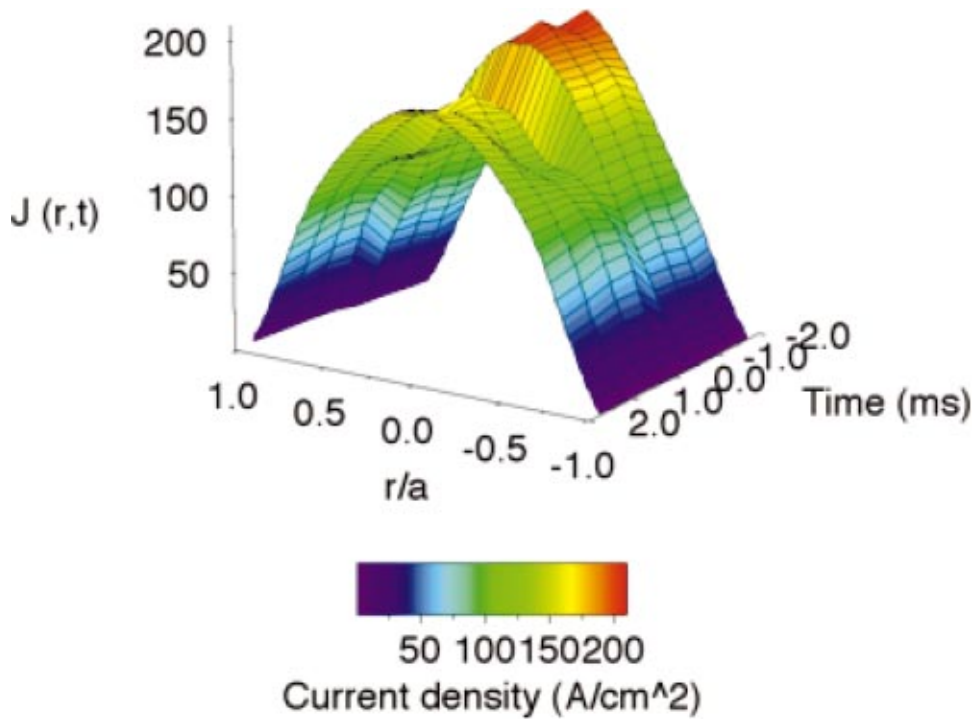


FIG. 8. (Color)  $J_{\parallel}$  decreases on axis and increases at the edge during a sawtooth crash.

eral factors could explain this increase. Fluctuations are measured to decrease during this period, leading to a decrease in driven dynamo current. Since the dynamo normally acts to suppress the core current, its absence could lead to an increase. Also, the core electron temperature is observed to increase, sometimes by a factor of 3. This will decrease the core resistivity and lead to higher currents on axis. Finally, new measurements of hard x-ray flux<sup>30</sup> indicate that the confinement of core runaway electrons increases during PPCD. These electrons can also carry significant amounts of current, leading to a drop in the effective resistivity in the core.

VI. SUMMARY AND CONCLUSIONS

Measurements of the toroidal and parallel current profiles, and the resulting changes in stability, have been obtained in the core of a reversed-field pinch. This data provides direct evidence of the hypothesis, suggested by previous measurements taken in the edge, that a sawtooth event relaxes the equilibrium toward a profile more stable to

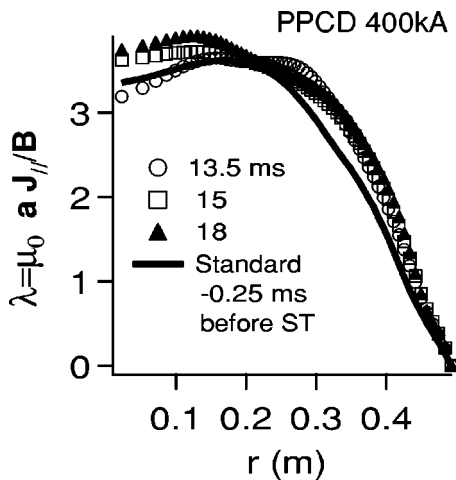


FIG. 9. A comparison of the  $\lambda$  profiles between standard and PPCD plasmas.  $\lambda$  first increases in the edge in PPCD ( $\sim 13.5$  ms) and then on-axis ( $\sim 15-18$  ms).

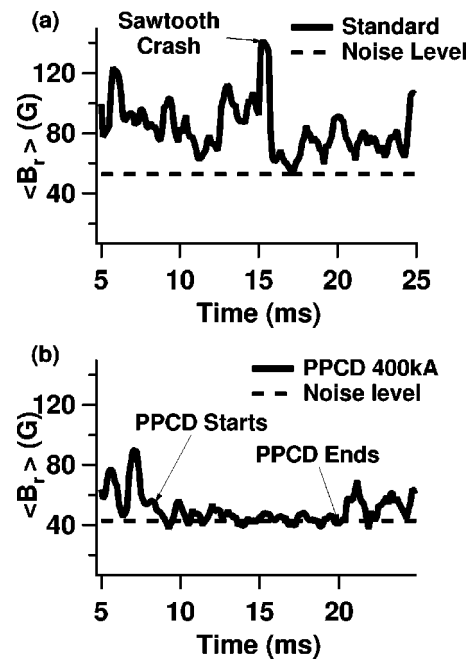


FIG. 10. Radial magnetic field fluctuations (measured by a line average on central chords) decrease during PPCD (b) compared to the standard case (a).

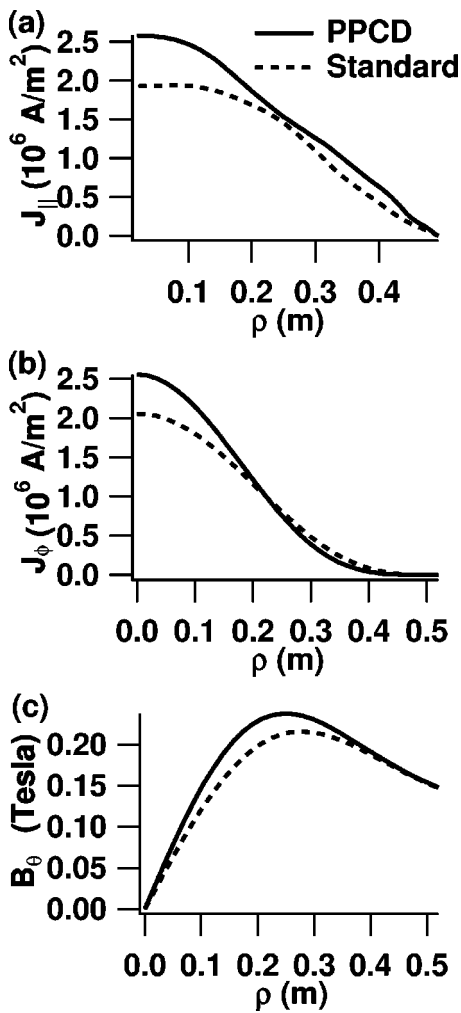


FIG. 11. A comparison of the (a) parallel current density, (b) toroidal current density, and (c) poloidal magnetic field between standard and PPCD plasmas.

tearing modes. The  $\lambda$  eigenvalue profile is observed to flatten after the crash, consistent with Taylor's conjecture. Radial magnetic field fluctuations and the toroidal electric field in the core increase at the crash suggestive of a nonlinear dynamo acting to relax the current profile. Poloidal flux decreases after the crash as it is converted to toroidal flux. Additionally, measurements in nonreversed discharges show similar phenomena at a reduced level.

In PPCD, the  $\lambda$  profile is seen to become flat over a larger volume of plasma. This is indicative of a more stable equilibrium, which is also shown by the decrease in core radial magnetic fluctuations during the PPCD pulse. The toroidal and parallel current profiles peak in the core. This could be caused by a drop in resistivity due to higher core  $T_e$ , the absence of antiparallel dynamo current, or an in-

crease in conductivity due to greater confinement of fast electrons and increased  $T_e(0)$ .

To provide direct evidence for the role of the dynamo in the plasma core, more direct measurements are needed. The radial and poloidal magnetic field fluctuations must be correlated with core velocity and current density fluctuations to measure the MHD and Hall dynamo terms in Ohm's law. This must be compared to the calculated parallel electric field in the core if a direct relationship between them is to be confirmed.

- <sup>1</sup>G. Fiksel, S. C. Prager, W. Shen, and M. Stoneking, Phys. Rev. Lett. **72**, 1028 (1994).
- <sup>2</sup>M. R. Stoneking, S. A. Hokin, S. A. Prager, G. Fiksel, H. Ji, and D. J. Den Hartog, Phys. Rev. Lett. **73**, 549 (1994).
- <sup>3</sup>J. B. Taylor, Rev. Mod. Phys. **58**, 741 (1986).
- <sup>4</sup>S. C. Prager, Plasma Phys. Controlled Fusion **41**, A129 (1999).
- <sup>5</sup>H. Ji, A. F. Almagri, S. C. Prager, and J. S. Sarff, Phys. Rev. Lett. **73**, 668 (1994).
- <sup>6</sup>D. J. Den Hartog, J. T. Chapman, D. Craig, G. Fiksel, P. W. Fontana, S. C. Prager, and J. S. Sarff, Phys. Plasmas **6**, 1813 (1999).
- <sup>7</sup>P. W. Fontana, D. J. Den Hartog, G. Fiksel, and S. C. Prager, Phys. Rev. Lett. **85**, 566 (2000).
- <sup>8</sup>J. S. Sarff, S. A. Hokin, H. Ji, S. C. Prager, and C. R. Sovinec, Phys. Rev. Lett. **72**, 3670 (1994).
- <sup>9</sup>M. R. Stoneking, N. E. Lanier, S. C. Prager, J. S. Sarff, and D. Sinityn, Phys. Plasmas **4**, 1632 (1997).
- <sup>10</sup>R. Bartiromo, P. Martin, S. Martini *et al.*, Phys. Plasmas **6**, 1830 (1999).
- <sup>11</sup>B. E. Chapman, T. M. Biewer, P. K. Chattopadhyay *et al.*, Phys. Plasmas **7**, 3491 (2000).
- <sup>12</sup>S. C. Prager, A. F. Almagri, S. Assadi *et al.*, Phys. Fluids B **2**, 1367 (1990).
- <sup>13</sup>T. M. Biewer, C. B. Forest, J. K. Anderson *et al.*, Phys. Rev. Lett. **91**, 045004 (2003).
- <sup>14</sup>S. Hokin, A. Almagri, S. Assadi *et al.*, Phys. Fluids B **3**, 2241 (1991).
- <sup>15</sup>J. K. Anderson *et al.*, "Dynamo free plasma in the reversed field pinch" (unpublished).
- <sup>16</sup>E. J. Caramana and D. R. Baker, Nucl. Fusion **24**, 423 (1984).
- <sup>17</sup>B. E. Chapman, J. K. Anderson, T. M. Biewer *et al.*, Phys. Rev. Lett. **87**, 205001 (2001).
- <sup>18</sup>N. E. Lanier, D. Craig, J. K. Anderson *et al.*, Phys. Rev. Lett. **85**, 2120 (2000).
- <sup>19</sup>C. R. Sovinec and S. C. Prager, Nucl. Fusion **39**, 777 (1999).
- <sup>20</sup>N. E. Lanier, D. Craig, J. K. Anderson *et al.*, Phys. Plasmas **8**, 3402 (2001).
- <sup>21</sup>Y. Jiang, D. L. Brower, and N. E. Lanier, Rev. Sci. Instrum. **70**, 703 (1999).
- <sup>22</sup>D. L. Brower, W. X. Ding, S. D. Terry *et al.*, Rev. Sci. Instrum. **74**, 1534 (2003).
- <sup>23</sup>Y. Jiang, D. L. Brower, and L. Zeng, Rev. Sci. Instrum. **68**, 902 (1997).
- <sup>24</sup>D. L. Brower, Y. Jiang, W. X. Ding, S. D. Terry, N. E. Lanier, J. K. Anderson, C. B. Forest, and D. Holly, Rev. Sci. Instrum. **72**, 1077 (2001).
- <sup>25</sup>W. X. Ding, D. L. Brower, S. D. Terry, D. Craig, S. C. Prager, J. S. Sarff, and J. C. Wright, Phys. Rev. Lett. **90**, 035002 (2003).
- <sup>26</sup>H. K. Park, Plasma Phys. Controlled Fusion **31**, 2035 (1989).
- <sup>27</sup>J. K. Anderson, Ph.D. thesis, University of Wisconsin, Madison, 2001.
- <sup>28</sup>V. Antoni, D. Merlin, S. Ortolani, and R. Paccagnella, Nucl. Fusion **26**, 1711 (1986).
- <sup>29</sup>D. L. Brower, W. X. Ding, S. D. Terry *et al.*, Phys. Rev. Lett. **88**, 185005 (2002).
- <sup>30</sup>R. O'Connell, D. J. Den Hartog, C. B. Forest *et al.*, Phys. Rev. Lett. **91**, 045002 (2003).